APPENDIX

Table of contents

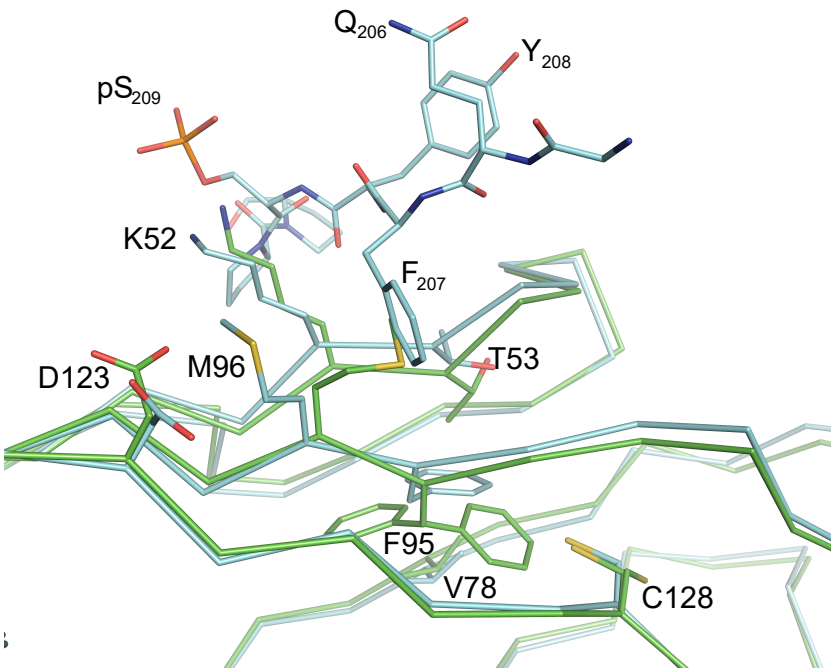

Appendix Figure S1: Structure comparison of the Phospho-FFAT-bound and unbound MSP domain of VAP-A.

Structure superposition the Phospho-FFAT-bound VAP-A (yellow) and the unbound VAP-A (pink). The main change between the FFAT-bound and unbound VAP-A is related to F95: in the unbound chains, the side chain of this residue seems to be disordered, but weak density can be seen for both the m-80 (chi angles: 306°, 284°) and t80 (chi angles: 192°, 88°) rotamers (with an associated double conformation of C128). In the chains bound to the peptide the side chain is well ordered in the m-80 rotamer, but slightly rotated away from C128 (chi angles: 277°, 277°). This orientation of the side chain places it between the side chains of T53 and V78, forcing T53 to move from the p rotamer (chi: 80°) to the t rotamer (chi: 175°). This rotamer change shifts the hydroxyl of the side chain to make a contact with the amide of A55, and it now no longer faces the solvent. Instead, the γ carbon of T53 now faces the side chains of Y_{208} and P_{210} of the STARD3 peptide (although the contacts are quite long). This also pushes the side chain of T53 causing a shift of the main chain positions of residues 51-54. This also shifts the side chain conformation of K52 which may influence how it can bind to the phosphoserine of the peptide. The conformation of M96 (and by association, D123) is also changed between the unbound and complexed forms of the domain. In the unbound form, M96 is in the mpp rotamer (chi angles: 293°, 77°, 70°) which shifts to the ttp rotamer (chi angles: 188°, 179°, 74°) when bound to the STARD3 peptide. This opens up the hydrophobic pocket which allows F_{207} of the peptide to bind. The change in conformation of D123 allows a hydrophobic interaction with M96. M96 also now forms hydrophobic contacts with the aliphatic part of the side chain of K52, which may stabilize its conformation. These residues are all conserved between human and rat VAP-A and adopt similar conformations in the structure of rat VAP-A in complex with the conventional FFAT motif of ORP1 (PDB ID: 1Z9O) with the different orientation of the peptide bringing A479 in to close proximity to the reoriented T53. It should be noted that in the unbound structure of rat VAP-A (PDB ID: 1Z9L) these residues are in similar conformations to the bound form, although a close examination of the electron density suggests that F95 may be partially disordered, and T53 is in a double conformation. M96 is also in a similar position to the complexed form, though it is making crystals contacts with the side chain of S100 in a symmetry related molecule, which may stabilize it in the ttp rotamer.

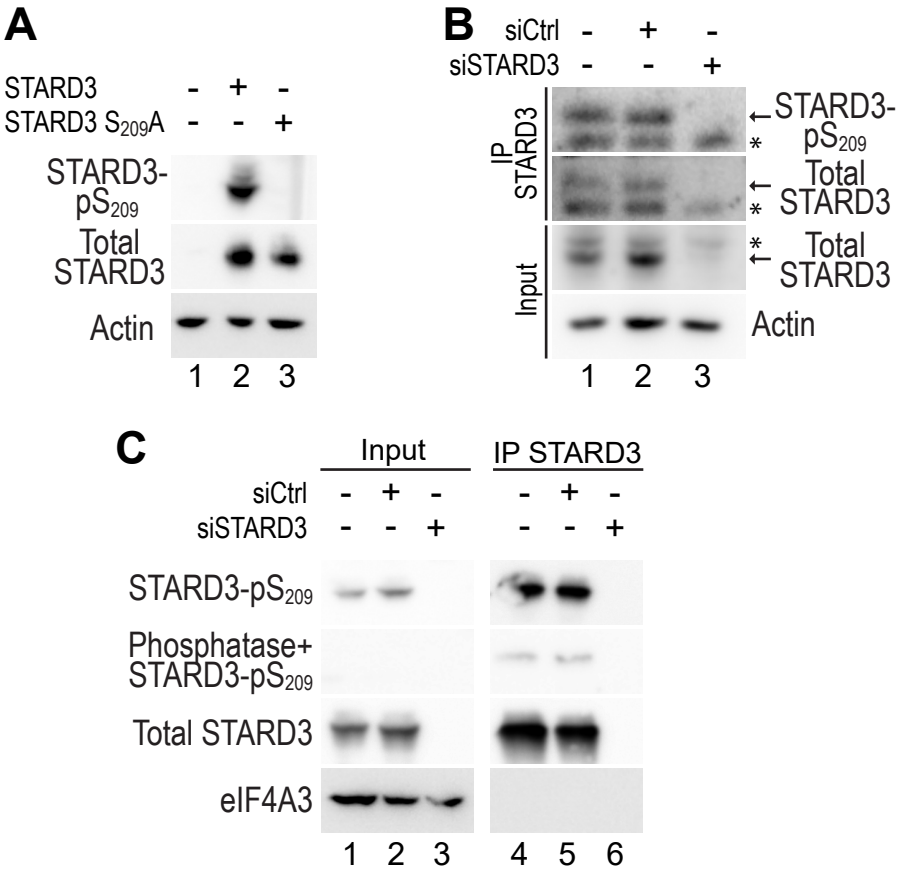

Appendix Figure S2: Analysis of the anti phospho-STARD3-pS$_{209}$ antibody recognizing STARD3 when phosphorylated on S$_{209}$.

A: Western blot analysis of protein extracts from HeLa cells transfected with constructs expressing wild-type STARD3 (lane 2), or the STARD3 S$_{209}$A mutant (lane 3). STARD3 was detected with an antibody recognizing both the phosphorylated- and non-phosphorylated protein (herein referred to as anti-STARD3) raised against a different part of the protein (the START domain of STARD3) and with the anti phospho-STARD3-pS$_{209}$ antibody. The anti-STARD3 antibody (total STARD3) recognized equally STARD3 and STARD3 S$_{209}$A proteins, while the anti-phospho-STARD3-pS$_{209}$ antibody recognized only the wild-type form of the protein. The anti-phospho-STARD3-pS$_{209}$ antibody is unable to detect the non phosphorylatable mutant STARD3 S$_{209}$A. Actin was used as a loading control.

B: Western blot analysis of endogenous STARD3 immunoprecipitated from HeLa cells. STARD3 was immunoprecipitated and detected using antibodies raised in mouse and rabbit, respectively. STARD3 was equally recognized by the anti-STARD3 and anti-phospho-STARD3-pS$_{209}$ antibodies thus showing that endogenous STARD3 is phosphorylated on S$_{209}$ in HeLa cells. HeLa cells transfected with siRNAs targeting STARD3 were used as control for the specificity of the antibodies (lane 3). *: aspecific band.

C: Western blot analysis of STARD3 phosphorylation in the HCC1954 breast cancer cell line that naturally expresses high amounts of STARD3. Endogenous STARD3 was immunoprecipitated from HCC1954 cells (lanes 1, 4), and HCC1954 cells transfected with a control siRNA (lanes 2, 5) or an siRNA targeting STARD3 (lanes 3, 6). STARD3 was immunoprecipitated and detected using antibodies raised in mouse and rabbit, respectively. STARD3 was detected with the anti-STARD3 (total STARD3) and the anti-phospho-STARD3-pS$_{209}$ antibodies in wild-type cells and in cells transfected with a control siRNA; no band was detected in cells silenced for STARD3. Calf Intestinal Phosphatase (CIP) treatment, that removes the phosphate group from phosphorylated residues, almost completely abolished the recognition of STARD3 by the anti-phospho-STARD3-pS$_{209}$ antibody. eIF4A3 was used as a loading control.

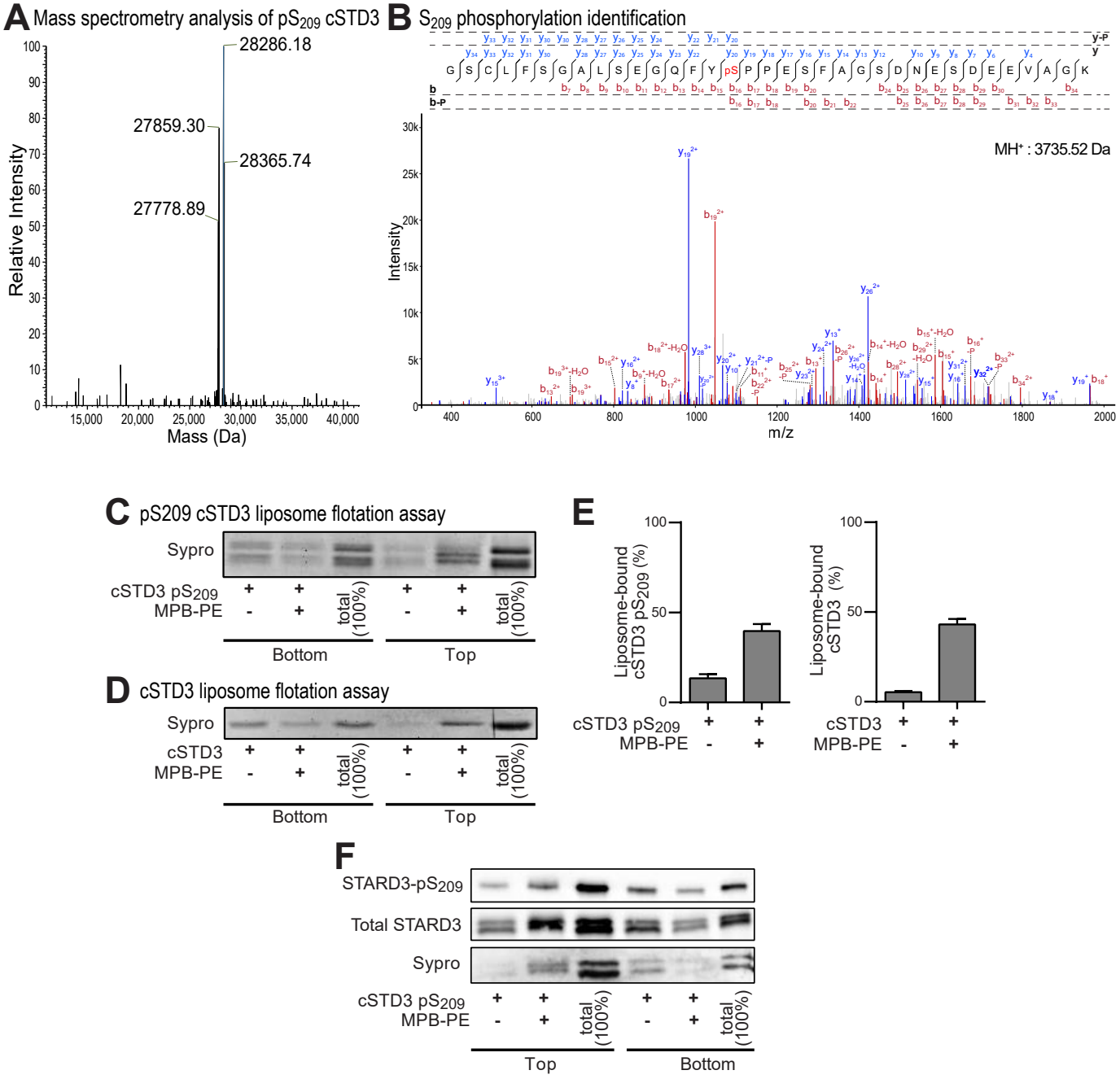

Appendix Figure S3: Characterization of cSTD3 and pS_{209} cSTD3 purified from E. coli

A: Mass spectrometry analysis of pS_{209} cSTD3 protein. Four major proteins are detected: two correspond to the non-phosphorylated (28,286.18 Da; theoretical MW: 28,287.98) and the phosphorylated (28,365.74 Da; theoretical MW: 28,367.96) cSTD3, respectively. The two other proteins correspond to the non-phosphorylated (27,778.89) and the phosphorylated (27,859.30 Da) cSTD3 exhibiting an N-terminal deletion of 5 residues (GSCLF) that was revealed by MS/MS analysis.

B: MS/MS spectrum of a peptide phosphorylated on S_{209}. The precursor peptide sequence and the different b (red) and y (blue) ions identified in the spectra are shown above. b and y ions with the highest intensity are labeled on the spectrum. Neutral mass losses of H_2O, NH_3, and H_3PO_4 (P) are indicated. The phosphosite probability determined with PhosphoRS was 96%.

C-E: Flotation assays: pS_{209} cSTD3 (C) and cSTD3 (D) (1.5 µM) were incubated with DOPC liposomes doped or not with 3 mol% MPB-PE (750 µM total lipids), in TN buffer for 10 minutes at 25°C, under agitation (850 rpm). After centrifugation, the top and bottom fractions were collected and analyzed by SDS-PAGE. The 100% lane was used to determine the fraction of cSTD3 present in the top fraction, thus bound to liposomes (E). Error bars show the S.E.M. from three independent experiments.

F: Analysis of the phosphorylation of pS209 cSTD3 bound to liposomes. cSTD3 pS_{209} (1.5 µM) was incubated with DOPC liposomes, containing or not 3 mol% MPB-PE (750 µM lipids) for 10 minutes at 25°C under agitation. After centrifugation, the top and bottom fractions were collected and analyzed by SDS-PAGE. Proteins were stained with Sypro Orange, and analysed by Western Blot using anti-STARD3 and anti-STARD3 pS_{209} antibodies.

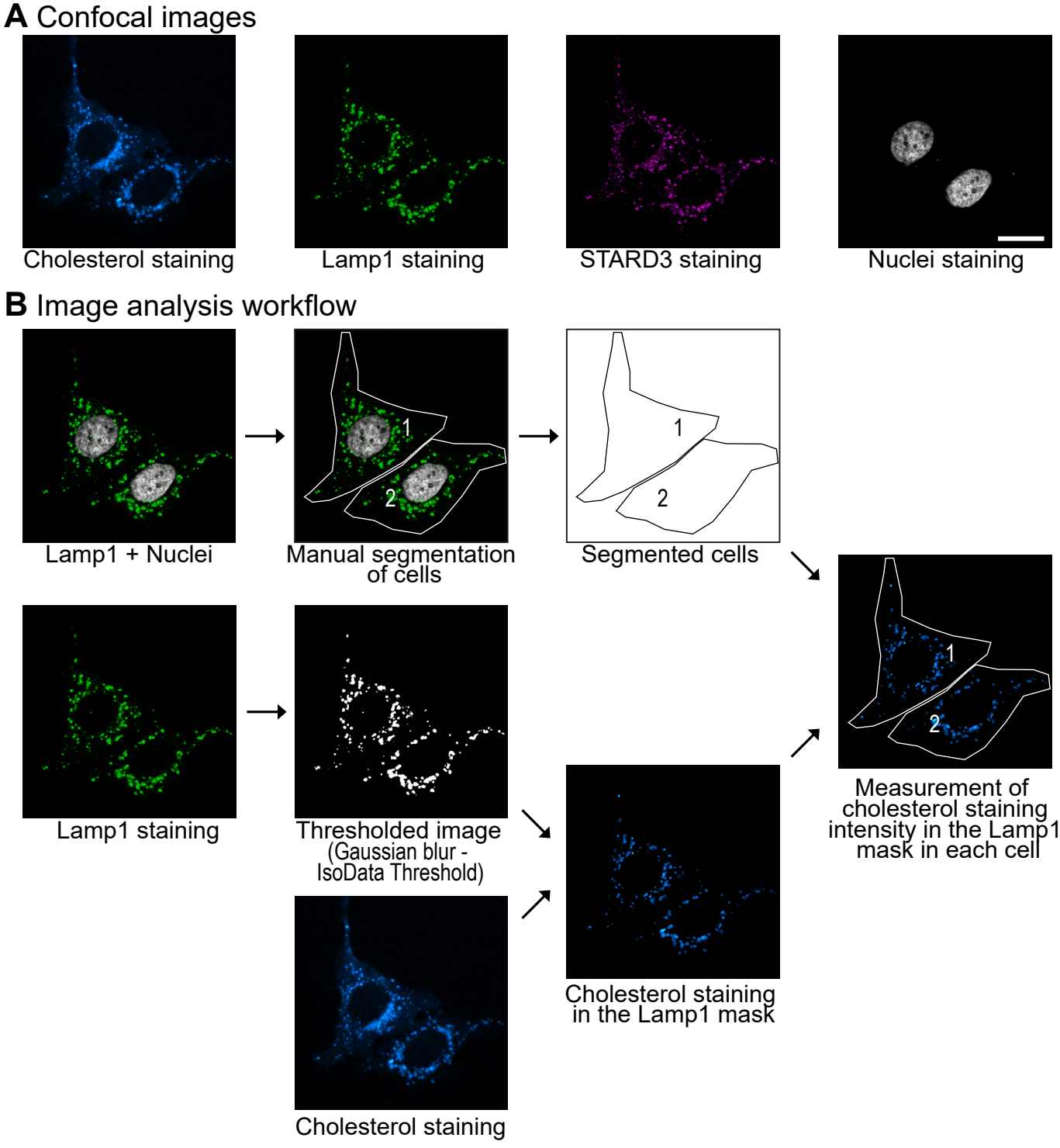

Appendix Figure S4: Filipin staining image analysis workflow

A: Cells stained with filipin, anti-Lamp1 and anti-STARD3 antibodies, and the DNA marker TOPRO-3 were imaged with a confocal microscope. Scale bar: 20 µm.

B: Images were analyzed with Fiji. Cell were manually segmented. Lamp1 staining images were treated with a Gaussian blur filter and thresholded (IsoData) to generate a mask corresponding to Lamp1-positive pixels. This mask was subsequently applied on the filipin staining image to generate an image in which pixels outside the Lamp1-mask were zeroed. This latter image, combined with cell segmentation, and the surface of the Lamp1-mask, allowed to calculate the mean filipin fluorescence intensity in Lamp1-positive pixels.

A

```
MOSPD2  322  VFKGPLLHISPAEELYFGSTESGEKKTLIVLTNVTKNIVAFKVRTTAPEKYRVKPSNSSCDPGA
VAP-A     9  AKHEQILVLDPPTDLKFKGPFTDVVTTNLKLRNPSDRKVCFKVKTTAPRRYCVRPNSGIIDPGS
VAP-B     2  AKVEQVLSLEPQHELKFRGPFTDVVTTNLKLGNPTDRNVCFKVKTTAPRRYCVRPNSGIIDAGA

MOSPD2  386  SVDIVVSPHG--GL-TVSAQDRFLIMAAEMEQSSGTGPAELTQFWKEVPRNKVMEHRLRCHTV 445
VAP-A    73  TVTVSVMLQPFDYDPNEKSKHKFMV QTIFAP-PNTS---DMEAVWKEAKPDELMDSKLRCVFE 131
VAP-B    66  SINVSVMLQPFDYDPNEKSKHKFMV QSMFAP-TDTS---DMEAVWKEAKPEDLMDSKLRCVFE 124
```

B

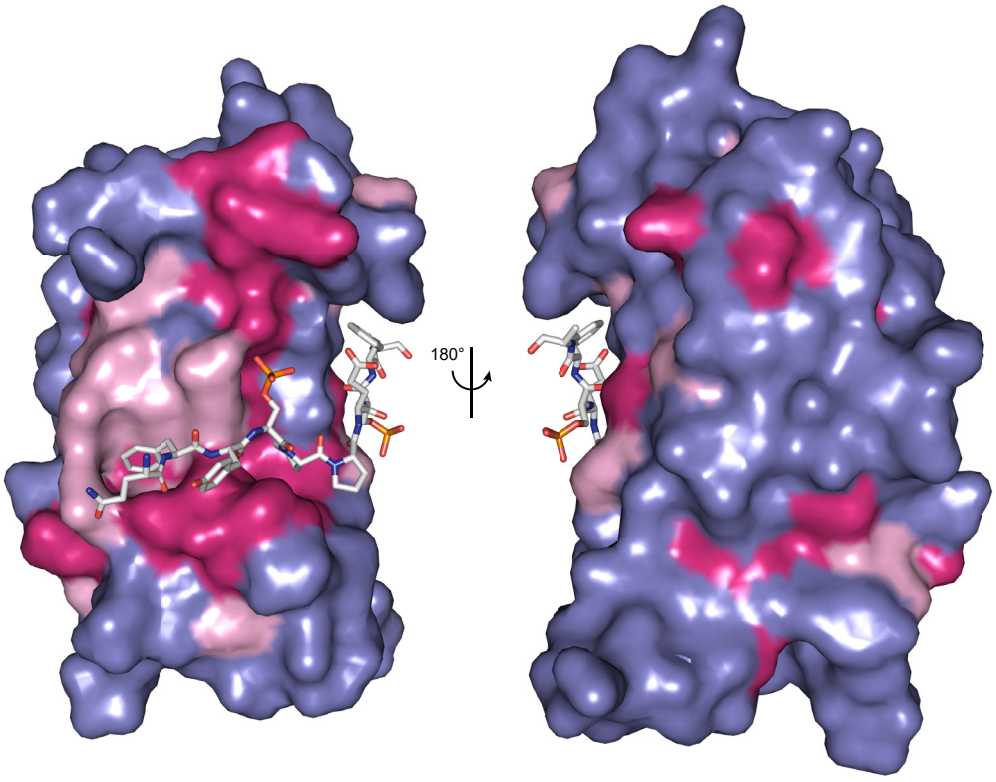

Appendix Figure S5: Sequence conservation between VAP-A, VAP-B and MOSPD2

A: Sequence alignment of the MSP domains of human MOSPD2, VAP-A, and VAP-B. Numbers refer to amino acid positions. Identical and conserved residues between the three proteins are labeled in magenta and pink, respectively. Sequences were aligned with ClustalW (Larkin et al, 2007) and formatted with Jalview (Waterhouse et al, 2009).
B: Structure of the MSP domain of MOSPD2 in complex with a Phospho-FFAT. Identical and conserved residues with VAP-A and VAP-B are labeled in red and pink, respectively.